Nanochem Res 8(1): 71-77 Winter 2023

RESEARCH PAPER

Magnetic, optical and carbon monoxide gas sensing properties of a facile solid state fabricated Bi_2O_3 nanomaterial

Younes Hanifehpour** [*], **Mehdi Abdolmaleki

Department of chemistry, Sayyed Jamaleddin Asadabadi University, Asadabad, Iran

ARTICLE INFO

Article History:
Received 01 Dec 2022
Accepted 22 Dec 2022
Published 30 Jan 2023

Keywords:
Rietveld
Solid State
Magnetic Property
CO gas sensing

ABSTRACT

A Bi_2O_3 nanomaterial was fabricated by a facile and low temperature solid state method using a basic bismuth nitrate raw compound at 400 ˚C and 14 h. Rietveld analysis data indicated that α-Bi_2O_3 was crystallized well in monoclinic crystal system with the space group of $P12_1/c1$. The morphology of the synthesized material was studied by field emission scanning electron microscope (FESEM). The direct band gap energy (Eg) value was calculated by ultraviolet – visible (UV-Vis) spectroscopy. The peaks at 400 – 550 cm^{-1} are assigned to oxygen – metal – oxygen (O-M-O) vibrations. The data showed that the Eg of the synthesized material was about 2.2 eV. In addition, the vibrating-sample magnetometer (VSM) analysis data confirmed that the synthesized sample had ferromagnetic behavior. Further, gas sensing property of the synthesized Bi_2O_3 nanomaterial for carbon monoxide gas was studied, and the data confirmed the good sensitivity of the prepared sensor at low CO concentrations.

How to cite this article
Hanifehpour Y., Abdolmaleki M., Magnetic, optical and carbon monoxide gas sensing properties of a facile solid state fabricated Bi2O3 nanomaterial. Nanochem Res, 2023; 8(1): 71-77 DOI: 10.22036/ncr.2023.01.007

INTRODUCTION

Alpha bismuth trioxide (α-Bi_2O_3) is an environmentally-friendly material [1]. Bi_2O_3 is a semiconductor with various physical and chemical properties including high refractive index, good photoconductive response, and high oxygen-ion conductivity. The E_g value of the α Bi_2O_3 is 2.85 eV [2]. There are some polymorphs of bismuth trioxide including α-Bi_2O_3, β-Bi_2O_3, γ-Bi_2O_3, δ-Bi_2O_3, ε-Bi_2O_3, and ω-Bi_2O_3 that are stable based on temperature. The stable crystal phase in low temperature is monoclinic α-Bi_2O_3 [3, 4, 5]. Bi_2O_3 has been studied extensively, and it has different applications in electrical ceramics, fuel cells, gas sensors, superconductors, optical coatings, supercapacitors, energy storage, and photocatalysts [6]. Furthermore, several methods have reported the fabrication of Bi_2O_3 such as solution [7,8], solution combustion [9], solvothermal [10], hydrothermal [11], laser ablation [12], microwave [13], sol–gel [14], pyrolysis [15], thermal decomposition [16,17], electrodeposition [18], thermal oxidation [19], chemical vapor deposition [20], green synthesis [21], and solid state with air annealing [22]. Solid state method is a useful and scalable route which can prepare nanomaterials with high purity and large amount without using any liquid solvent [23]. Additionally, there are several studies reporting the sensing application of nanomaterials [24-27].

The present work reports the facile, one-step, and low-temperature solid state fabrication of Bi_2O_3 nanomaterials. To our knowledge, there is no report about the preparation of the nanomaterials under the present conditions. The crystallographic data of the fabricated nanomaterials are obtained by Rietveld analysis. Moreover, the characterization, morphology as well as optical, magnetic, and

* Corresponding Author Email: *younes.hanifehpour@gmail.com*

electrochemical properties of the synthesized samples are investigated by XRPD, FESEM, FTIR, UV-Vis and VSM analyses. The main goal of the present work is the synthesis of new classes of Bi_2O_3 nanomaterial by the low-temperature solid state route. Besides, this paper describes the application of Bi_2O_3 nanomaterials as a CO gas sensor. Our results suggest that the obtained material has remarkable sensitivity as CO gas sensor.

MATERIALS AND METHODS

Experimental method

All of the used raw materials such as $Bi_5O(OH)_9(NO_3)_4$ were purchased from Sigma Aldrich Company, were of analytical grade (99%) and used without further purification. The characterization and identification of the crystal-phase type fabricated nanopowders was conducted by X-ray powder diffractometer D5000 (Siemens AG, Munich, Germany) using CuK_α radiation with the deviation of ±0.02°. *FullProf* software was employed to study the Rietveld analysis. The morphology and elemental analysis of the obtained materials were examined by a Philips XL30 scanning electron microscope (Philips, Amsterdam, Netherlands). A Tensor 27 spectrometer (Bruker Corporation, Germany) with the deviation of ±2 cm^{-1} was utilized to record the FTIR spectrum. Recording the absorption spectra and calculation of the band gap energies were carried out by Analytik Jena Specord 40 (Analytik Jena AG Analytical Instrumentation, Jena, Germany) apparatus with the deviation of ±2 nm. In addition, the magnetic property of the samples was studied by a vibrating sample magnetometer (VSM, Model 7400-LakeShore) with the deviation of ±0.001 H(Oe). The gas sensing experiments were conducted in a home-made testing system (a cylindrical stainless steel chamber with a volume of 300 mL) which is called sensing analysis system in research institute of petroleum industry (SAS-RIPI).

The crystallite size data of the fabricated Bi_2O_3 nanomaterials is calculated by the Scherrer equation.

The parameter X-ray density (ρ_x) is calculated by the following formula:

SSA is calculated by ρ_{xrd} and D data according to the below equation [28]:

Preparation of Bi_2O_3 nanomaterial

Pure and doped Bi_2O_3 nanomaterials were synthesized by a one-step solid state method involving thermal decomposition of bismuth nitrate raw material in normal atmospheric condition. In this case, 0.5 g (0.34 mmol) of $Bi_5O(OH)_9(NO_3)_4$ (MW=1462 g mol^{-1}) was ground in a ceramic crucible and heated in one step at 400 ˚C for 24 h in a preheated electric furnace. Afterwards, the sample was cooled down to room temperature in the furnace.

Preparation and evaluation of the sensor

To fabricate gas sensor, the prepared Bi_2O_3 powder was ground into tiny-flour, and then blended with TX100 with the weight ratio of 3:1 to form a homogeneous paste. Then, the pastes were coated on alumina substrates (1mm×1 mm). Gold shoulder electrodes were coated on the surface substrates by the sputtering technique, followed by drying at room temperature. Before testing, the sensors were aged at 400 ºC for 12 h to improve repeatability and stability.

All sensors were pre-heated at different operating temperatures for 30 min. When the resistance reached a constant value, the test chamber was opened to let the gas in. As the air and target gas flowed through the test chamber, the corresponding resistances of the sensor in air (Ra) and target gas (Rg) were measured. In this paper, the sensitivity of the gas response (S) was defined as the ratio of sensor's resistance in air to that in target gas (S = Ra/Rg). The response and recovery times were defined as the time required for a change in response to reach 90 % of the equilibrium value after injecting and removing the detected gas, respectively. During the test, the operating temperature range was set at 200-350 ºC, and the relative humidity was 40 %.

RESULTS AND DISCUSSIONS

Characterization

The synthesized Bi_2O_3 sample was characterized by the X-ray diffraction method. The XRPD pattern is presented in Fig. 1. *FullProf* program employing profile matching with constant scale factors was used to perform the structural analysis of the as-fabricated sample. Red lines are the observed peaks intensities (Y_{obs}) and the black ones are the calculated data (Y_{calc}). The blue line denotes the difference: $Y_{obs} - Y_{calc}$. According to Fig. 1, the bars presented above the green line correspond to α-Bi_2O_3 with the crystal structure of monoclinic with space group of $P12_1/c1$ [1-5]. The miller indices are 24.55, 25.74, 26.75, 27.41, 32.98, 46.18

Table 1. Cell parameter and counts values of the as-prepared materials.

Sample	2θ	$B_{1/2}$	a	B	c	ρx	SSA (m^2/g)	Counts
Bi_2O_3	27.4062	0.003685	5.84385	8.15800	7.51099	0.86	1.8	133

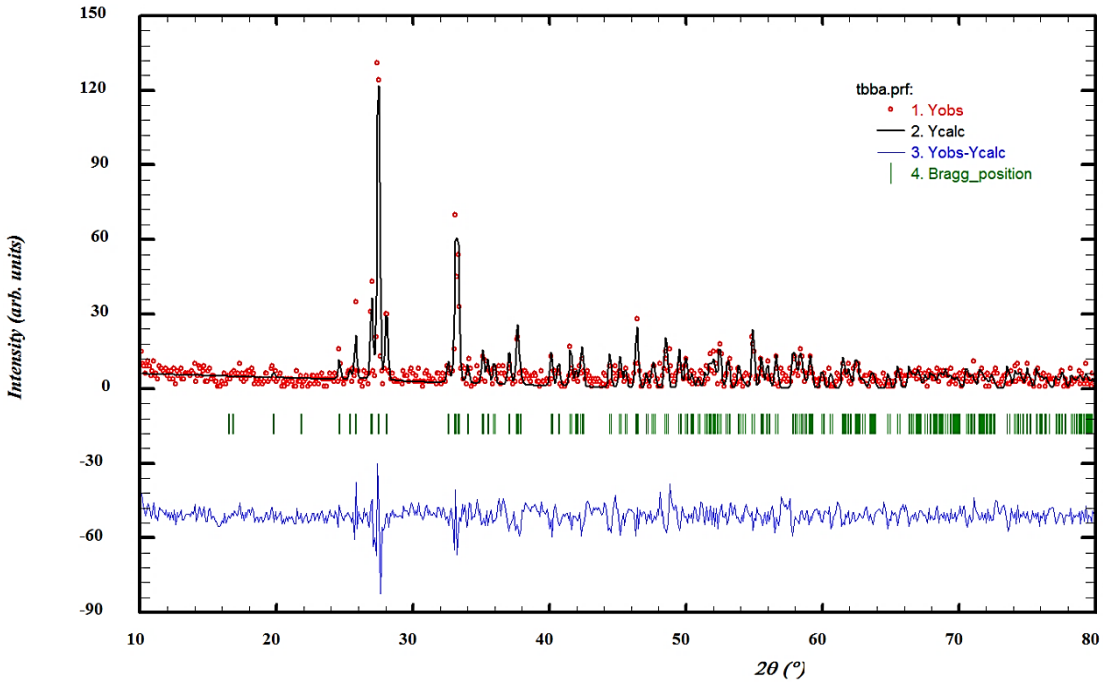

Fig. 1. XRPD patterns of the as-prepared Bi_2O_3 nanomaterials.

are (-102), (002), (-112), (101), (-211), and (-223) for the main peaks.

The crystallographic data of the obtained sample was calculated for monoclinic crystal system. The crystallite size (D) of the fabricated Bi_2O_3 nanomaterial is reported in Table 1. In the Scherrer equation, D is the crystalline sample's entire diameter thickness; the X-ray diffraction wavelength is λ (0.154 nm); the Scherrer constant is K (0.9); $B_{1/2}$ denotes the full width at half of its maximum intensity (FWHM) of the certain used peak, and θ is the half diffraction angle of the peak. In this formula to calculate ρx, M is the molecular weight of Bi_2O_3 (MW=466 $gmol^{-1}$); N is the Avogadro number; Z is the number of formula unit per unit cell for Bi_2O_3 (Z=4) and *a, b, c* are lattice parameters. The specific surface area (SSA) per lattice volume is a physical property that can affect physical and chemical behavior.

Morphology analysis

Fig. 2 presents FESEM images of the as-prepared nanomaterial. As can be seen from the images, the morphology of the sample is particles. It is clear from the images that the homogeneity of particles morphology is high. Further, the particles have close sizes and most of the them have sizes smaller than 20 nm. However, there are some particles with larger sizes around 80-100 nm.

Magnetic property

The magnetic property of the fabricated sample was investigated by VSM analysis to understand the magnetic behavior of the synthesized powder. The magnetic hysteresis (M-H) curve of the as-prepared Bi_2O_3 is shown in Figs. 3a and b. The plots reveal the evidence that the nanomaterials manifest ferromagnetic behavior at room temperature. According to Fig. 3a, the saturation magnetization (M_s) value is 0.01 emu/g. Furthermore, the data indicates that the compound keeps the magnetization in zero fields when the external magnetic field was applied. Remanence magnetization, M_r, is the magnetization strength

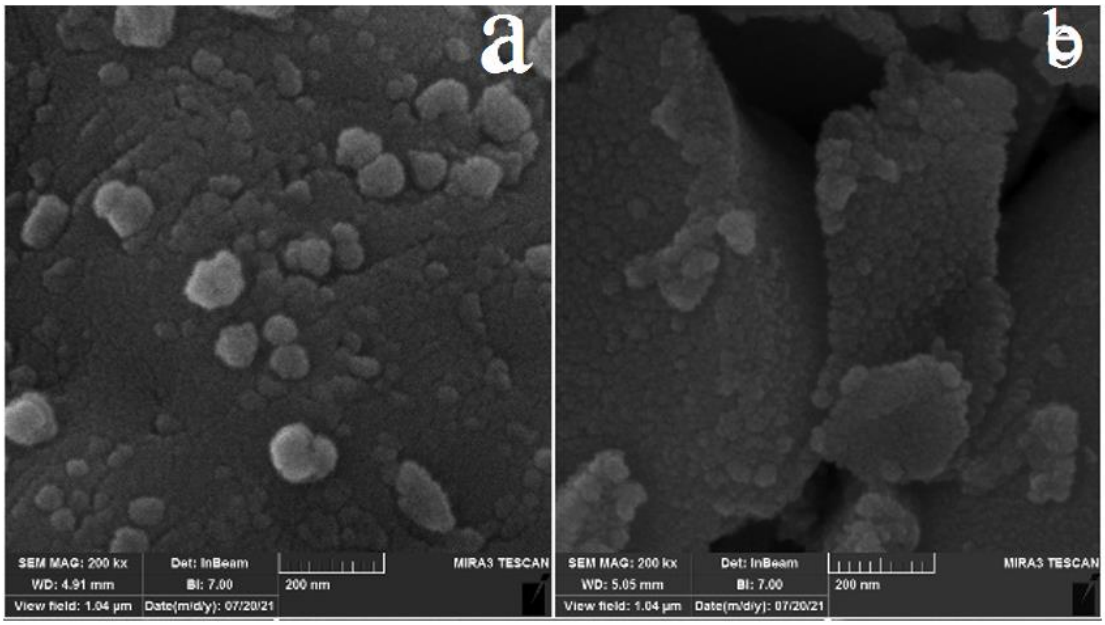

Fig. 2. FESEM images of the as-prepared samples

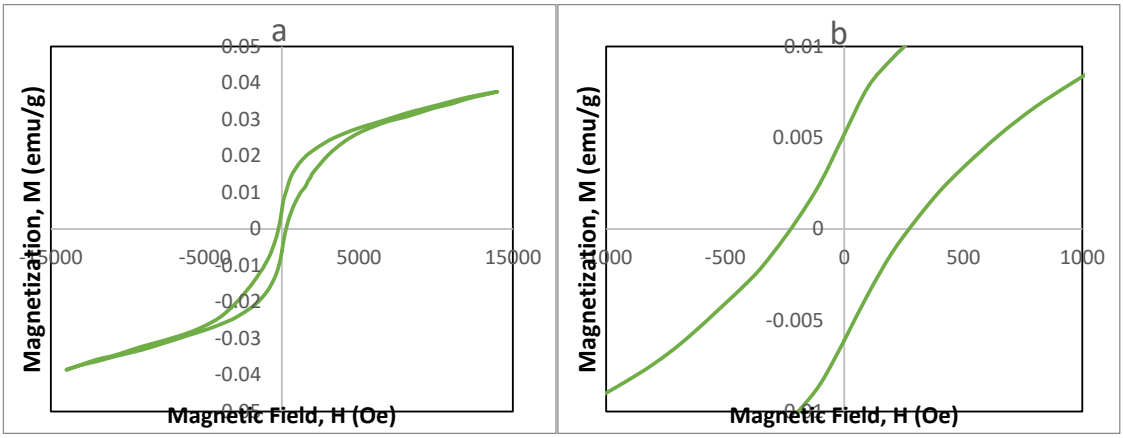

Fig. 3. Room temperature M–H curves of the as-synthesized nanomaterials

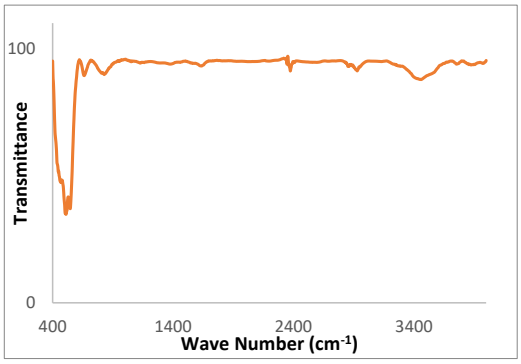

Fig. 4. FTIR spectrum of the as-prepared nanomaterial.

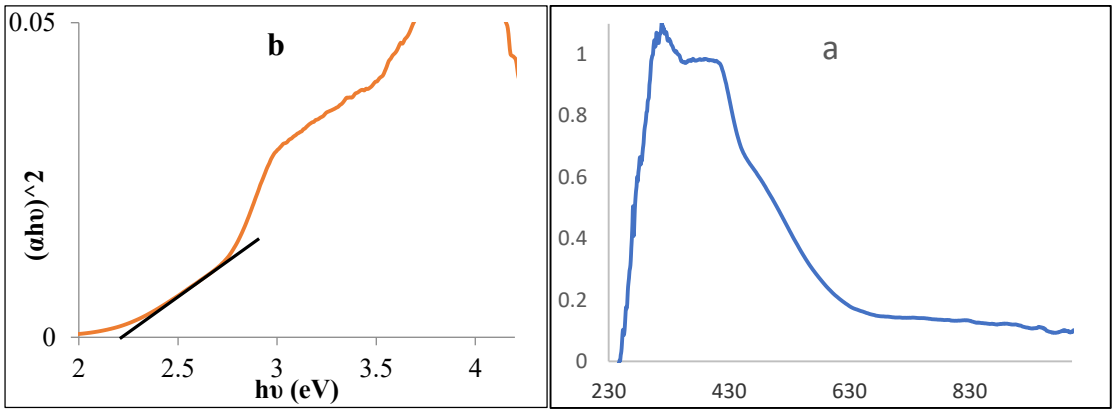

Fig. 5. a) UV-Vis spectrum and b) direct band gap energy of the as-prepared nanopowder.

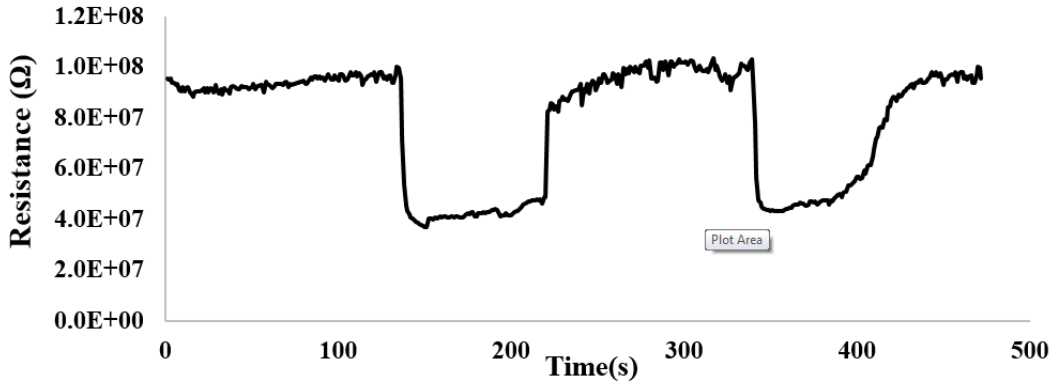

Fig. 6. Resistance response of pure Bi_2O_3 sensors to 150 ppm CO gas at 200 °C

in which the magnetization is retained when the external magnetic field is zero (H = 0) [29]. By magnifying the loop (Fig. 3b), the data indicated that the most saturation remanence (M_r) is 0.008. The squareness ratio ($M_{rs} = M_r/M_s$) magnitude is calculated by the ratio of remanence and saturation magnetization. When a particle is distributed isotropically and uniformly magnetized without intergrain interactions, the material will have a squareness ratio below 0.5 which confirms the formation of multi-domain structure when the exchange coupling between adjacent grains takes place. In the present work, it was found that M_{rs} is 0.4. Therefore, the data demosntrate that there is no preferred direction in magnetization for the fabricated compound.

Optical Property

FTIR spectrum of the as-prepared nanomaterial is shown in Fig. 4. The general peaks for all samples are at about 512, 546, 620, 650, 770, 850, 1650, 2300, 2900 and 3400 cm^{-1}. In general, metal oxides show absorption bands below 1000 cm^{-1}. The peaks at 400 – 550 cm^{-1} are assigned to oxygen – metal – oxygen (O-M-O) vibrations. Additionally, the bands located at 546, 620, 650, 770 and 850 cm^{-1} are assigned to the stretching vibration modes of Bi–O bonds of BiO_6 octahedron [30,31]. Moreover, the peak located at 646 cm^{-1} is attributed to Bi-O vibration [32,33], and the peaks at 1650 and 3400 cm^{-1} also correspond to the physically adsorbed H_2O [34]. The peaks at 2300 and 2900 cm^{-1} can be attributed to carbonate impurity vibrations [35].

UV-Vis absorption spectrum of the fabricated nanomaterial is shown in Fig. 5a. The E_g plot of the sample is also presented in Fig. 5b. According to the UV-Vis absorption data, it is found that the nanomaterial possesses a typical strong absorption edge at about 500 nm. The light absorption in the region suggesting a fantastic photoactive

property under blue light irradiation. Besides, a wide absorption region from 330 – 430 nm exists in the absorption plot. The relation between the absorption coefficient and incident photon energy can be written as $(\alpha h\nu)^2 = A(h\nu - Eg)$ for direct band gap energy. In this equation, A and Eg are a constant value and direct band gap energy, respectively [36]. To measure the Eg value, the linear part of the curve to the energy axis is extrapolated. Fig. 6b indicates that the synthesized material shows a strong band structure at 2.30 eV.

Carbon monoxide sensing properties

To investigate the performance of bismuth oxide sensor for detecting carbon monoxide, the nanostructure of Bi_2O_3 nanomaterial was synthesized. According to Fig. 6, it can be seen that the Bi_2O_3 has good sensitivity to CO gas at low levels of carbon monoxide at 200 °C.

CONCLUSION

The present work reported the facile solid-state synthesis of Bi_2O_3 nanomaterial. Rietveld analysis data confirmed the high purity of the obtained nanomaterial. FESEM images indicated that the homogeneity of particles morphology was high. In addition, the particles had close sizes and most of the particles had sizes smaller than 20 nm. It was found that the synthesized material showed strong band structure at 2.30 eV. The magnetic property data confirmed the ferromagnetic behavior of the synthesized materials. No preferred direction in the magnetization was found for the synthesized sample. Satisfactory CO gas sensing was confirmed by using Bi_2O_3 as sensor at 200 °C sensing medium.

ACKNOWLEDGMENT

This work is funded by Sayyed Jamaleddin Asadabadi University Research Grant

CONFLICT OF INTEREST

The authors declare they have no conflict of interest for the present work.

REFERENCES

1. Alshehri MA, Aziz AT, Trivedi S, Panneerselvam C. Efficacy of chitosan silver nanoparticles from shrimp-shell wastes against major mosquito vectors of public health importance. 2020;9(1):675-84. doi:10.1515/gps-2020-0062
2. Yanat M, Schroën K. Preparation methods and applications of chitosan nanoparticles; with an outlook toward reinforcement of biodegradable packaging. Reactive and Functional Polymers. 2021;161:104849. https://doi.org/10.1016/j.reactfunctpolym.2021.104849
3. Al-Zahrani SS, Bora RS, Al-Garni SM. Antimicrobial activity of chitosan nanoparticles. Biotechnology & Biotechnological Equipment. 2021;35(1):1874-80. 10.1080/13102818.2022.2027816
4. Trung TS, Tram LH, Van Tan N, Van Hoa N, Minh NC, Loc PT, et al. Improved method for production of chitin and chitosan from shrimp shells. Carbohydrate Research. 2020;489:107913. https://doi.org/10.1016/j.carres.2020.107913
5. Klongthong W, Muangsin V, Gowanit C, Muangsin N. Chitosan Biomedical Applications for the Treatment of Viral Disease: A Data Mining Model Using Bibliometric Predictive Intelligence. Journal of Chemistry. 2020;2020:6612034. 10.1155/2020/6612034
6. Aranaz I, Mengibar M, Harris R, Panos I, Miralles B, Acosta N, et al. Functional Characterization of Chitin and Chitosan. Current Chemical Biology. 2009;3(2):203-30. 10.2174/187231309788166415
7. Islam S, Bhuiyan MAR, Islam MN. Chitin and Chitosan: Structure, Properties and Applications in Biomedical Engineering. Journal of Polymers and the Environment. 2017;25(3):854-66. 10.1007/s10924-016-0865-5
8. Dash S, Kumar M, Pareek N. Enhanced antibacterial potential of berberine via synergism with chitosan nanoparticles. Materials Today: Proceedings. 2020;31:640-5. https://doi.org/10.1016/j.matpr.2020.05.506
9. Gadkari RR, Suwalka S, Yogi MR, Ali W, Das A, Alagirusamy R. Green synthesis of chitosan-cinnamaldehyde cross-linked nanoparticles: Characterization and antibacterial activity. Carbohydrate Polymers. 2019;226:115298. https://doi.org/10.1016/j.carbpol.2019.115298
10. Romainor ANB, Chin SF, Pang SC, Bilung LM. Preparation and characterization of chitosan nanoparticles-doped cellulose films with antimicrobial property. Journal of Nanomaterials. 2014;2014.
11. Abdallah Y, Liu M, Ogunyemi SO, Ahmed T, Fouad H, Abdelazez A, et al. Bioinspired Green Synthesis of Chitosan and Zinc Oxide Nanoparticles with Strong Antibacterial Activity against Rice Pathogen Xanthomonas oryzae pv. oryzae. Molecules [Internet]. 2020; 25(20). 10.3390/molecules25204795
12. Okafor V, Umenne C, Tabugbo B, Okonkwo C, Obiefuna J, Okafor U, et al. Potentiality of Diethylamine as Agent of Deproteination and Deacetylation in the Extraction of Chitosan from Scylla serrata Shell. Chemistry and Materials Research. 2020;Vol. 12:35-45. 10.7176/CMR/12-7-07
13. Teli MD, Sheikh J. Extraction of chitosan from shrimp shells waste and application in antibacterial finishing of bamboo rayon. International Journal of Biological Macromolecules. 2012;50(5):1195-200. https://doi.org/10.1016/j.ijbiomac.2012.04.003
14. Pakizeh M, Moradi A, Ghassemi T. Chemical extraction and modification of chitin and chitosan from shrimp shells. European Polymer Journal. 2021;159:110709. https://doi.org/10.1016/j.eurpolymj.2021.110709
15. Agoha EEC, editor Biomaterials from Periwinkle Shells: Composition and Functional Properties. World Congress on Medical Physics and Biomedical Engineering 2006; 2007 2007//; Berlin, Heidelberg: Springer Berlin Heidelberg.
16. Isa M. Extraction and Characterization of Chitin and Chitosan from Mussel Shell. Civil and Environmental Research. 2013;3:108-14.
17. Okoya A, Akinyele A, Amuda O, Ofoezie E. Chitosan Grafted

Modified Maize Cob for Removal of Lead And Chromium from Wastewater. Ethiopian Journal of Environmental Studies and Management. 2016;8:881. 10.4314/ejesm.v8i2.3S

18. Wijayadi LJ, Rusli TR. Characterized and synthesis of chitosan nanoparticle as nanocarrier system technology. IOP Conference Series: Materials Science and Engineering. 2019;508(1):012143. 10.1088/1757-899X/508/1/012143
19. Rashid MU, Bhuiyan MKH, Quayum ME. Synthesis of Silver Nano Particles (Ag-NPs) and their uses for Quantitative Analysis of Vitamin C Tablets. Dhaka University Journal of Pharmaceutical Sciences. 2013;12(1):29-33. 10.3329/dujps.v12i1.16297
20. Abdallah Y, Ogunyemi SO, Abdelazez A, Zhang M, Hong X, Ibrahim E, et al. The Green Synthesis of MgO Nano-Flowers Using Rosmarinus officinalis L. (Rosemary) and the Antibacterial Activities against Xanthomonas oryzae pv. oryzae. BioMed Research International. 2019;2019:5620989. 10.1155/2019/5620989
21. Jeyaraman DM, R.Vignesh, N.Sumathi. EXTRACTION, CHARACTERIZATION AND APPLICATIONS OF CHITOSAN FROM FISH SCALES. 2017. 10.21884/IJMTER.2017.4131.Q8NJR
22. Udenni Gunathilake TMS, Ching YC, Ching KY, Chuah CH, Abdullah LC. Biomedical and Microbiological Applications of Bio-Based Porous Materials: A Review. Polymers [Internet]. 2017; 9(5). 10.3390/polym9050160
23. Yahya EB, Jummaat F, Amirul AA, Adnan AS, Olaiya NG, Abdullah CK, et al. A Review on Revolutionary Natural Biopolymer-Based Aerogels for Antibacterial Delivery. Antibiotics [Internet]. 2020; 9(10). 10.3390/antibiotics9100648
24. Britto Hurtado R, Cortez-Valadez M, Flores-Lopez NS, Flores-Acosta M. Agglomerates of Au-Pt bimetallic nanoparticles: synthesis and antibacterial activity. Gold Bulletin. 2020;53(2):93-100. 10.1007/s13404-020-00277-y
25. Murugan K, Jaganathan A, Suresh U, Rajaganesh R, Jayasanthini S, Higuchi A, et al. Towards Bio-Encapsulation of Chitosan-Silver Nanocomplex? Impact on Malaria Mosquito Vectors, Human Breast Adenocarcinoma Cells (MCF-7) and Behavioral Traits of Non-target Fishes. Journal of Cluster Science. 2017;28(1):529-50. 10.1007/s10876-016-1129-1
26. Kannan RRR, Arumugam R, Ramya D, Manivannan K, Anantharaman P. Green synthesis of silver nanoparticles using marine macroalga Chaetomorpha linum. Applied Nanoscience. 2013;3(3):229-33. 10.1007/s13204-012-0125-5
27. Murugan K, Anitha J, Suresh U, Rajaganesh R, Panneerselvam C, Aziz AT, et al. Chitosan-fabricated Ag nanoparticles and larvivorous fishes: a novel route to control the coastal malaria vector Anopheles sundaicus? Hydrobiologia. 2017;797(1):335-50. 10.1007/s10750-017-3196-1
28. Chen Q, Jiang H, Ye H, Li J, Huang J. Preparation, Antibacterial, and Antioxidant Activities of Silver/Chitosan Composites. Journal of Carbohydrate Chemistry. 2014;33(6):298-312. 10.1080/07328303.2014.931962
29. Sathyavathi R, Krishna MB, Rao SV, Saritha R, Rao DN. Biosynthesis of Silver Nanoparticles Using Coriandrum Sativum Leaf Extract and Their Application in Nonlinear Optics. Advanced Science Letters. 2010;3(2):138-43. 10.1166/asl.2010.1099
30. Dara PK, Mahadevan R, Digita PA, Visnuvinayagam S, Kumar LRG, Mathew S, et al. Synthesis and biochemical characterization of silver nanoparticles grafted chitosan (Chi-Ag-NPs): in vitro studies on antioxidant and antibacterial applications. SN Applied Sciences. 2020;2(4):665. 10.1007/s42452-020-2261-y
31. Zahedi S, Safaei Ghomi J, Shahbazi-Alavi H. Preparation of chitosan nanoparticles from shrimp shells and investigation of its catalytic effect in diastereoselective synthesis of dihydropyrroles. Ultrasonics Sonochemistry. 2018;40:260-4. https://doi.org/10.1016/j.ultsonch.2017.07.023
32. Kalaivani R, Maruthupandy M, Muneeswaran T, Hameedha Beevi A, Anand M, Ramakritinan CM, et al. Synthesis of chitosan mediated silver nanoparticles (Ag NPs) for potential antimicrobial applications. Frontiers in Laboratory Medicine. 2018;2(1):30-5. https://doi.org/10.1016/j.flm.2018.04.002
33. Sonseca A, Madani S, Rodríguez G, Hevilla V, Echeverría C, Fernández-García M, et al. Multifunctional PLA Blends Containing Chitosan Mediated Silver Nanoparticles: Thermal, Mechanical, Antibacterial, and Degradation Properties. Nanomaterials [Internet]. 2020; 10(1). 10.3390/nano10010022
34. Liu X, Wang T, Chow LC, Yang M, Mitchell JW. Effects of Inorganic Fillers on the Thermal and Mechanical Properties of Poly(lactic acid). International Journal of Polymer Science. 2014;2014:827028. 10.1155/2014/827028